5f states in UGa2 probed by x-ray spectroscopies

Kolomiets, A. V.; Paukov, M.; Valenta, J.; Chatterjee, B.; Andreev, A. V.; Kvashnina, K. O.; Wilhelm, F.; Rogalev, A.; Drozdenko, D.; Minarik, P.; Kolorenc, J.; Richter, M.; Prchal, J.; Havela, L.;

Originally published:

July 2021

Physical Review B 104(2021)4, 045119

DOI: https://doi.org/10.1103/PhysRevB.104.045119

5*f* states in UGa_2 probed by x-ray spectroscopies

A. V. Kolomiets,[1,2] M. Paukov,[1] J. Valenta,[1] B. Chatterjee,[3] A. V. Andreev,[3] K. O. Kvashnina,[4,5] F. Wilhelm,[6] A. Rogalev,[6] D. Drozdenko,[1] P. Minarik,[1] J. Kolorenč,[3] M. Richter,[7,8] J. Prchal,[1] and L. Havela[1]

[1]*Charles University, Faculty of Mathematics and Physics, Department of Condensed Matter Physics, Ke Karlovu 5, 121 16 Prague 2, Czech Republic*

[2]*Department of Physics, Lviv Polytechnic National University, 12 Bandera Str., 79013 Lviv, Ukraine*

[3]*Institute of Physics, Czech Academy of Sciences, Na Slovance 2, 182 21 Prague 8, Czech Republic*

[4]*Institute of Resource Ecology, Helmholtz-Zentrum Dresden-Rossendorf, 01313 Dresden, Germany*

[5]*The Rossendorf Beamline at the European Synchrotron (ESRF), 38043 Grenoble, France*

[6]*The European Synchrotron (ESRF), 38000 Grenoble, France*

[7]*Leibniz IFW Dresden, Helmholtzstraße 20, 01069 Dresden, Germany*

[8]*Dresden Center for Computational Materials Science (DCMS), TU Dresden, 01062 Dresden, Germany*

(Received 5 January 2021; revised 23 March 2021; accepted 7 June 2021; published xxxxxxxxxx)

The 5*f*-based ferromagnet UGa_2 with the Curie temperature $T_C = 125$ K was investigated by x-ray absorption spectroscopy (XAS) and x-ray magnetic circular dichroism (XMCD) experiments at the U–$M_{4,5}$ and Ga–*K* edges. The position of the U–M_4 white line, determined in the high-energy resolution fluorescence detection XAS, suggests that UGa_2 is neither a localized $5f^2$ nor an itinerant system with 5*f* occupancy close to $n_{5f} = 3$. The analysis of the acquired $M_{4,5}XANES$ and $XMCD$ spectra indicates the 5*f* occupancy close to 2.5 and a large orbital magnetic moment of the uranium 5*f* states (3.18 μ_B) that is partly compensated by the antiparallel spin moment (1.31 μ_B). Thus, the total 5*f* magnetic moment of 1.87 μ_B is obtained, which is smaller than the known bulk magnetization of 3.0 μ_B per formula unit, while the magnetic moments of the Ga atoms are negligible. Several methods based on density-functional theory were applied and the obtained results were compared with XAS spectral features, the Sommerfeld coefficient of the electronic specific heat, and the size of the U moments and 5*f* occupancies. A clear correlation is revealed between the U–M_4 white-line position of three metallic uranium compounds and the calculated uranium ionicity. It is demonstrated that only electronic structure methods taking appropriate care of orbital magnetism and related atomic multiplet effects can successfully describe all considered properties.

DOI: 10.1103/PhysRevB.00.005100

I. INTRODUCTION

A leading theme of actinides research in solid state is the Mott transition on the 5*f* electronic states, taking place in pure elements between Pu and Am. Higher occupancies of the 5*f* states increase the total electron-electron correlation energies inside the 5*f* shell, and the 5*f* electrons eventually decrease the total energy by abandoning the formation of bonding states in favor of localized atomiclike states, which minimize the correlation energies. Enhanced actinide-actinide distances in compounds can suppress the bonding character even more, shifting the Mott transition towards less occupied 5*f* states. However, focusing on uranium as the most studied actinide, we see that the complete localization of the 5*f* states is a very rare event. Among intermetallics, there is only one binary compound, UPd_3, where the 5*f* localization has compelling evidence by photoelectron spectroscopy and a low density of states at the Fermi level, $g(E_F)$, to which the localized 5*f* states do not contribute [1,2]. One of the few binary compounds, which can be roughly classified as close to the localization regime, is UGa_2. It crystallizes in the hexagonal AlB_2-type crystal structure (space group $P6/mmm$, $a = 4.213$ Å and $c = 4.012$ Å) [3], one of the most simple binary structures, in which Ga atoms effectively separate U atoms, increasing the shortest U-U distance to more than 4.0 Å. Such a large distance can generally explain the formation of U magnetic moments and their ferromagnetic ordering below $T_C = 125$ K [3]. The size of U moments, $\mu_U = 3.0(2)\ \mu_B$ determined by neutron diffraction study [4] corresponds to the low-temperature magnetization in magnetic fields along [100], which is the easy-magnetization direction. Both T_C and μ_U are higher than typical values found for other ferromagnetic uranium intermetallics, although μ_U is still lower than 3.25 μ_B/U or 3.33μ_B/U expected for $5f^2(U^{4+})$ or $5f^3(U^{3+})$ configurations in the intermediate coupling scheme [5].

The electronic contribution to the specific heat with a Sommerfeld coefficient $\gamma = 11$ mJ/mol K^2 [6] is not much enhanced over the value 5 mJ/mol K^2 for the analog without 5*f* electrons, $LaGa_2$ [7], and points to the absence of large 5*f* contributions to the density of electronic states at the Fermi level. One reason for this could naturally be the 5*f* localization. Localized 5*f* states were suggested by earlier density-functional theory (DFT) [8] and crystal electric-field calculations [9], although there remained an uncertainty whether they are of $5f^2$ or $5f^3$ type. The opposite, that is, itinerant character of the 5*f* states, was deduced from photoemission studies [10]. Finally, the results of magnetoresistance

and de Haas–van Alphen experiments [6] could not be convincingly explained by either the localized or itinerant model if calculating the Fermi surface in the local spin-density approximation (LSDA).

A certain indicator of localization is the observed response of magnetism to the volume compression achieved by hydrostatic pressure. For a typical band system, external pressure leads to a broadening of bands and a related reduction of the density of states at the Fermi level, leading to suppression of magnetism as the value of the Stoner product, $I \cdot g(E_F)$, where I is the Stoner parameter and $g(E_F)$ is the density of states at the Fermi level, is reduced below 1. UGa_2 behaves very differently, as the Curie temperature T_C first strongly increases (up to 154 K at $p = 14$ GPa) and then turns down [11]. Such type of behavior can be understood as insensitivity of the 5*f* moments to pressure below a certain limit. The compression initially increases the exchange coupling, probably by enhanced hybridization with non-*f* states. At higher pressure, roughly above 10 GPa, the moments start to be reduced, and although the coupling strength still increases, the ferromagnetism is fading in a strongly nonlinear way. Should the magnetic interactions involve fully localized states, the external pressure would have little effect on the magnetic moments and their ordering temperatures.

Determination of T_C under pressure could be performed on the basis of electrical resistivity data, which is definitely easier than determination of magnetization. To investigate the latter, the technique of x-ray magnetic circular dichroism (XMCD) can be in principle performed with a sample located in a diamond-anvil cell. The XMCD signal at the *M* edge of uranium can give, using the sum rules, the spin and orbital part of U magnetic moments. However, the strong absorption of several keV photons in diamond makes this experiment challenging and the XMCD experiment was so far performed and analyzed for the ambient pressure only. Here we describe results of a simpler x-ray absorption spectroscopy (XAS) experiment, accomplished as the pressure study of the $M_{4,5}$ absorption edges at room temperature and without magnetic field, reaching $p = 7.2$ GPa. Although the current instrumentation could not reach the critical pressure range, spreading above 10 GPa, the results give an interesting characterization of UGa_2.

The position of the *M* absorption edge carries important information about the 5*f* occupancy, which, as we mentioned above, is one of the unresolved issues. To accurately determine the position of the edge, we performed an x-ray absorption experiment using a high-energy resolution fluorescence detection (HERFD) mode at room temperature.

II. EXPERIMENTAL DETAILS

The measurements were performed on UGa_2 single crystals grown by the Czochralski technique. A twinning with approximately 2° misalignment of the *a* axis between different grains was found. For spectroscopy experiments, the crystal was cut and polished to provide a flat plane perpendicular to the *a* axis.

The high-resolution absorption measurements were performed at room temperature at the beamline ID26 [12] of the European Synchrotron Radiation Facility (ESRF) in Grenoble. The incident energy was selected using the ⟨111⟩ reflection from a double Si crystal monochromator. Rejection of higher harmonics was achieved by three Si mirrors at angles of 3.0, 3.5, and 4.0 mrad relative to the incident beam. X-ray absorption near-edge structure (XANES) spectra were measured in the high-energy resolution fluorescence detection mode using an x-ray emission spectrometer [13,14]. The sample, the analyzer crystal, and the photon detector (silicon drift diode) were arranged in a vertical Rowland geometry. The uranium HERFD XAS spectra at the M_4 edge were obtained by recording the maximum intensity of the U-M_β emission line (≈3337 eV) as a function of the incident energy. The emission energy was selected using the ⟨220⟩ reflection of five spherically bent Si crystal analyzers (with 1 m bending radius) aligned at 75° Bragg angle. The paths of the incident and emitted x-rays through air were minimized in order to avoid losses in intensity due to absorption. The intensity was normalized to the incident flux. A combined (incident convoluted with emitted) energy resolution of 0.4 eV was obtained as determined by measuring the full width at half maximum (FWHM) of the elastic peak. The present data are not corrected for self-absorption effects. The analysis shown in this work is based on comparison of the energy position of the main transitions at the U–M_4 edge which is only little affected by self-absorption effects. The energy calibration was in each case related to a preceding UO_2 measurement using identical experimental conditions. Therefore, the relative accuracy between all the spectra shown can be taken as better than 0.1 eV.

The conventional XANES and XMCD spectra were measured at the beamline ID12 [15] of ESRF. The source is the first harmonic of the helical electromagnet/permanent magnet hybrid undulator, which provides high flux of circularly polarized x-ray photons and allows for reversing the helicity of the x-rays at each energy point. After monochromatization with a double-crystal Si(111) monochromator, the rate of circular polarization is reduced to about 0.35 at the M_5 edge and to 0.45 at the M_4 absorption edge. For the ambient pressure measurements performed at $T = 15$ K we used an oriented millimeter-sized single crystal of UGa_2, where the magnetic easy axis (the [100] direction) was collinear with the k vector of the x-ray beam. The XANES spectra were recorded using the total fluorescence yield detection mode in backscattering geometry for parallel $\mu_+(E)$ and antiparallel $\mu_-(E)$ alignments of the photon helicity with respect to a 3 T external magnetic field applied along the beam direction. The XANES spectra for right and left circularly polarized x-ray beams were then corrected for self-absorption effects, which have been proven to work very well in the case of U multilayers [16], and for incomplete circular polarization rates of incident x-ray photons. The U edge-jump intensity ratio M_5/M_4 was then normalized to 3:2 according to the statistical edge-jump ratio (defined as the ratio between the occupation numbers for the two spin-orbit-split core levels $j = 3/2$ and 5/2). This statistical U edge-jump intensity ratio M_5/M_4 is very close to the value (1.57) tabulated in the XCOM tables by Berger *et al.* [17]. A deviation of ±10% in the M_5/M_4 XAS edge-jump normalization (ratio of 1.5) would affect the branching ratio $B = I_{M5}/(I_{M5} + I_{M4})$ by ±2.5% and similarly the occupation numbers of the $j = 5/2$ and $j = 7/2$

subshells $n^{5f}{}_{5/2}$ and $n^{5f}{}_{7/2}$. Further details concerning the analysis of uranium M-edges spectra in uranium magnetic compounds can be found elsewhere [18]. The XMCD spectra $\mu_+(E)-\mu_-(E)$ were obtained as the difference of the corrected XANES spectra. To make sure that the final XMCD spectra are free of any experimental artifacts, measurements were also performed for the opposite direction of the applied magnetic field.

For the high-pressure measurements performed at $T =$ 300 K, a dedicated high-pressure diamond-anvil cell (DAC) with a He gas-driven membrane optimized for the tender x-ray range has been used [19]. The DAC consisted of an asymmetric diamond-anvil configuration, in which a fully perforated diamond, with a culet diameter of 600 μm, and a hole diameter of 100 μm (front anvil) was complemented by a 50-μm-thick diamond disk to minimize the x-ray absorption. The back anvil was a full diamond with the same culet diameter of 600 μm. The gasket was made of stainless steel. A single crystal of $80 \times 80 \times 30\,\mu m^3$ was loaded inside the cell, and He gas was used as the pressure-transmitting medium. The pressure was measured *in situ* using the luminescence of a ruby chip. Using the specific DAC, we could reach a pressure up to $p = 7.2$ GPa. The XANES signal from the sample was collected in the backscattering geometry, through the thin diamond window, using a Si photodiode. As focalization system, a set of 2D parabolic Be lenses with the curvature radius of 0.2 mm together with a pair of pinholes having an aperture of 0.8 mm was used. High-order harmonics of the undulator emission were rejected using a pair of vertically focusing mirrors.

III. COMPUTATIONAL DETAILS

The electronic structure of UGa_2 was modeled by several approaches based on DFT as implemented in two different relativistic all-electron full-potential codes. This comprises the local spin-density approximation, the generalized gradient approximation (GGA), and a combination of LSDA with the Hubbard model constructed for the uranium 5f electrons. The Hubbard model was approximately solved using the static mean-field theory (the LSDA+U method) and the dynamical mean-field theory (the LDA+DMFT method).

Apart from LDA+DMFT, all mentioned methods suffer from an incomplete description of orbital magnetism that stems from orbital-dependent self-interaction present in the local or semilocal approximations to DFT [20]. For this reason and in view of the importance of the orbital magnetism in uranium compounds, orbital-polarization corrected (OPC) [21,22] GGA was used to model the magnetic properties in another calculation.

It should be mentioned that the LSDA+U method may suffer from a multitude of metastable solutions. A possible way to exhaust the solution space is occupation matrix control [23]. Here, this computationally expensive approach was not applied since, in a metal with relatively broad (> 1 eV) bands, the possibility of metastable states is largely reduced in comparison with narrow-band insulators.

A. WIEN2K

The WIEN2K code implements the linearized augmented plane-wave (LAPW) method and its extensions. The core states (U up to 5d, Ga up to 3p) are evaluated in the muffin-tin sphere by numerically exact integration of the Kohn-Sham-Dirac equations. All higher-lying states are considered as the valence states, for which the method combines a scalar-relativistic description with spin-orbit coupling added in a second variational step. See Ref. [24] and references therein for further details. Most of the calculations were performed at the experimental lattice geometry ($a = 4.213$ Å, $c = 4.020$ Å) with the following parameters: the radii of the muffin-tin spheres were $R_{MT}(\mathrm{U}) = 2.80\,a_B$ for the uranium atoms and $R_{MT}(\mathrm{Ga}) = 2.25\,a_B$ for the gallium atoms, and the plane-wave cutoff K_{max} was set by $R_{MT}(\mathrm{Ga}) \times K_{max} = 10$. The equation of state (Table I) and the properties under pressure (see Fig. 5) were obtained with smaller radii, $R_{MT}(\mathrm{U}) = 2.45\,a_B$ and $R_{MT}(\mathrm{Ga}) = 2.05\,a_B$, necessitated by the reduced interatomic distances in the compressed lattice. The default basis set containing local orbitals for semicore states (U 6s and 6p, and Ga 3d) was used in all cases. Integrals in the reciprocal space were computed with a modified tetrahedron method with Blöchl corrections using an $18 \times 18 \times 17$ sampling of the full Brillouin zone.

TABLE I. Computed equilibrium volume, lattice constants, and bulk modulus (LSDA and LSDA+U methods) compared to the experimental data. The row labeled as LSDA* corresponds to a metastable state (a local minimum of the total energy) that is 0.37 eV/ UGa_2 higher than the global minimum. All calculations are for the ferromagnetic state with moments along the [100] direction.

Method	V_0(Å^3)	a_0(Å)	c_0(Å)	c_0/a_0	K (GPa)
LSDA	52.73	4.61	2.87	0.622	109
LSDA*	57.59	4.15	3.86	0.931	99
LSDA+U (2 eV)	59.70	4.15	4.00	0.964	99
Experiment	61.79	4.21 [3]	4.02 [3]	0.954	100 ± 8 [49]

The LSDA calculations were performed with the Perdew-Wang (PW92) parametrization of the exchange-correlation functional [25]. The Coulomb parameter U entering the LSDA+U functional was varied in the range 0–2 eV, the exchange parameter J was fixed to 0.4 eV, and the fully localized limit was taken for the double-counting correction.

The LDA+DMFT method was applied in the variant described in Ref. [26]: the *nonmagnetic* (spin-restricted) band structure calculated in the local-density approximation with the WIEN2K code was represented by a tight-binding model in the basis of the maximally localized Wannier functions (with uranium 7s, 5f, 6d, and 7p character, and gallium 4s and 4p character) [27,28], and the DMFT self-energy for the uranium 5f states was computed by solving the auxiliary impurity model in a reduced Fock space using the Lanczos method. The impurity model consisted of 14 spin-orbitals for the uranium 5f shell and 42 spin-orbitals representing the hybridization of the 5f shell with its environment. The off-diagonal hybridization, induced by noncommutativity of the hexagonal symmetry at the uranium site with the spin-orbit coupling, was taken into account. The Coulomb interaction among the 5f electrons was considered in its full spherically symmetric form parametrized by four Slater integrals, $U = F_0 = 2.0$ eV, $F_2 = 7.09$ eV, $F_4 = 4.60$ eV, and $F_6 = 3.36$ eV. The first integral is at the upper limit of the range explored with the

LSDA+U method; the other three correspond to the atomic Hartree-Fock values calculated for the $U^{3+}(5f^3)$ ion and then reduced to 80% to account for screening [29].

In our LDA+DMFT implementation, the ferromagnetic solution is induced by introducing a small symmetry-breaking magnetic field to the impurity model that is removed again after a few iterations of the self-consistency cycle. The tight-binding model stays frozen in its initial form derived from the nonmagnetic LDA, and the spin (and orbital) polarization is introduced only to the 5f states by means of the polarized self-energy. Since no charge self-consistency is attempted, the exchange field induced by 5f electrons and experienced by the 6d electrons, and the exchange field induced by 6d electrons and experienced by 5f electrons, both correspond to the nonmagnetic state and are thus, incorrectly, absent from our description of the electronic structure. We address this deficiency by introducing an empirical exchange splitting Δ_{fd} to the 5f shell, analogously to the earlier computational investigations of rare-earth systems [30,31]. The magnitude of this splitting can be estimated as $\Delta_{fd} \approx I_{fd} m_d$, where m_d is the magnetic moment due to 6d electrons and I_{fd} is the intra-atomic exchange integral. The magnetic moment can be approximated by its LSDA value, $m_d \approx 0.24\,\mu_B$; the exchange integral can be estimated by atomic calculations, $I_{fd} \approx 0.15\,\text{eV}/\mu_B$ [32]. This yields $\Delta_{fd} \approx 35$ meV. This small exchange splitting has a sizable effect on the magnetic moments, but its influence on the spectral properties is negligible. Note that the total exchange splitting in LSDA is approximately 1 eV, the dominant contribution being naturally the 5f–5f exchange, which is incorporated in the self-energy in the LDA+DMFT method. The calculations employing the estimated exchange splitting Δ_{fd} are denoted as LDA+DMFT*.

The double-counting correction in the LDA+DMFT calculations was treated as a tunable parameter chosen to maintain the 5f filling near the LSDA value, that is, to simulate charge self-consistency. This condition implies the double-counting correction $\approx$ 3.0 eV for $U = 2.0\,\text{eV}$. We used the same value in the LDA+DMFT* variant as well, since the double-counting (Hartree) term should not depend on the exchange splitting.

The Sommerfeld coefficient γ was evaluated using the Fermi-liquid formula

$$\gamma = \frac{\pi^2 k_B^2}{3}\left[\frac{g_f(E_F)}{Z_f} + g_{\text{non-}f}(E_F)\right],$$

where $g_f(E_F)$ is the density of the uranium 5f states at the Fermi energy E_F, $g_{\text{non-}f}(E_F)$ is the density of all other states at the Fermi energy, and $Z_f < 1$ is the average quasiparticle weight for the 5f states that is evaluated from the DMFT self-energy as suggested in Ref. [33]. In static approximations, such as LSDA and LSDA+U, the quasiparticle weight equals 1.

B. FPLO

The full-potential local-orbital (FPLO) code [34] uses a four-component (Dirac) implementation of the relativistic Kohn-Sham equations. The presented results were obtained with fplo-18.00-52 by employing the Perdew-Burke-Ernzerhof (PBE) implementation of GGA [35]. The same experimental structure data as in the WIEN2K calculations were used for UGa_2. For the other two systems studied, experimental structure data were used as well: USn_3 (space group 221, $a = 4.603$ Å) and UPd_3 (space group 194, $a = 5.769$ Å, $c = 9.640$ Å). Integrations in the reciprocal space were carried out with a linear tetrahedron method including Blöchl corrections on a mesh of $24 \times 24 \times 24$ ($18 \times 18 \times 18$) intervals in the full Brillouin zone for UGa_2 and USn_3 (UPd_3). Densities of states (DOS) of UGa_2 were evaluated with a finer mesh of $48 \times 48 \times 48$ intervals. The default FPLO valence basis set was used which comprises uranium 5d, 5f, 6s, 6p, 6d, 6f, 7s, 7p, 7d, and 8s states as well as gallium 3s, 3p, 3d, 4s, 4p, 4d, 5s, and 5p states. All lower-lying states are treated as core states.

The data for charge distributions (ionicities and occupation numbers) and for the absolute position of the $3d_{3/2}$ level, which are hardly influenced by magnetic order, were obtained by nonmagnetic GGA calculations. In addition, the effect of the core hole on the $3d_{3/2}$ level position was modeled on a $2 \times 2 \times 2$ supercell with 24 atoms, reciprocal space mesh $7 \times 7 \times 7$, and one U atom constrained to host a static 3d hole, while the electronic structure was allowed to relax.

In the context of charge distribution, two comments are of importance: (1) Each electronic structure method makes use of an individual technique to analyze ionicities and occupation numbers. For example, the WIEN2K code uses a separation into spheres around each nucleus and interstitial volumes. The FPLO code uses a projection onto overlapping local (atomiclike) orbitals, which yields comparable but not equal occupation numbers as the WIEN2K code. (2) A special feature of the projection onto overlapping orbitals is the possibility to distinguish net and overlap contributions to the occupation numbers. The net contributions relate to the product of two orbitals at the same atom, while the overlap contributions relate to the product of two orbitals at different atoms, i.e., they can be used as a measure of hybridization or delocalization. The sum of net and overlap occupations are called gross occupation numbers, which in turn sum up to the total electron number. The ionicity discussed below is defined as the difference between the electron number of the respective neutral atom and the calculated total electron number of that atom.

Magnetic properties were evaluated by means of GGA and GGA+OPC calculations. For the latter, the original OPC version suggested by Eriksson *et al.* [21] was used, since it should be more appropriate than later spin-dependent versions for the present case of strong spin-orbit coupling.

IV. EXPERIMENTAL RESULTS

The x-ray absorption at the M edge captures the electron excitations from the U 3d states. While M_4 corresponds to the transition $3d_{3/2} \rightarrow 5f_{5/2}$, M_5 to $3d_{5/2} \rightarrow 5f_{5/2,7/2}$. The $3d_{3/2}$ and $3d_{5/2}$ are split by the spin-orbit coupling energy of 173 eV. Hence, the M_4 edge at 3.72 keV probes the unoccupied part of the $5f_{5/2}$ states, while the M_5 edge at 3.56 keV probes the empty part of both the $5f_{5/2}$ and $5f_{7/2}$ states. Using circularly polarized x-rays with different helicity, one can derive the total orbital and spin polarization of occupied 5f states, that is, the orbital and spin magnetic moments, expressed in terms

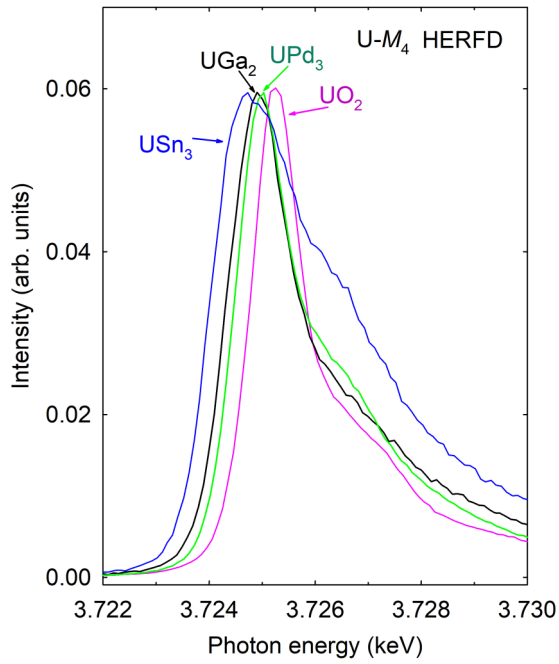

FIG. 1. U–M_4 edge of UGa_2 (black line) compared with spectra of UPd_3, UO_2, and USn_3, all from Ref. [36].

of relative dichroic signal integrated over the energy scale. The short 3d hole lifetime, causing the energy resolution to be principally limited to 4 eV, is not a limiting factor for the dichroic experiment, as intensities are integrated over a larger energy window. However, we can extract additional information from small energy shifts of the absorption maxima, which can reflect the bonding and/or electrostatic conditions in analogy to, e.g., energies of photoelectron spectra of core-level lines. The net shift of M edge towards lower energies with increasing 5f occupancy can be related to an enhanced Coulomb 3d-5f repulsion. On the other hand, the 5f delocalization should have the opposite effect if the 5f occupancy is maintained, reflecting larger distance between the 3d and 5f orbitals. The 4-eV resolution would not allow determination of such subtle effects. For such purpose, a specific deexcitation channel can be chosen if the energy analysis of fluorescence photons is available. Choosing a "slow" deexcitation process removes the lifetime limitation. In other words, the short lifetime of the 3d hole is not an issue anymore if we use for example its filling via an intermediate state with a 4f hole. The realization of such high-energy resolution fluorescence detection spectroscopy was used in this work, using the M_β detection energy for the M_4 line yielding the combined energy resolution 0.4 eV. The present work concentrated on the M_4 line, which is narrower and small energy shifts can be easier observed than for the M_5 line.

A. M_4-edge HERFD XAS experiment and preliminary discussion

HERFD XAS was the technique used to collect the data presented in Fig. 1, showing a detailed view of the M_4 edge. The spectrum of UGa_2 is compared with the spectra of UO_2, UPd_3, and USn_3 taken from Ref. [36], all collected using the same experimental conditions [36] and normalized to maximum intensity. The energies of the maxima certainly depend on the energy of the initial 3d states (initial state effect) with respect to the Fermi level and this must be the dominant effect if the 5f states form a band intersected by the Fermi energy. As a final-state effect, progressing localization, similarly to the formation of a Mott gap in oxides, splits off the 5f spectral density from the Fermi level, and an additional energy has to be paid to reach the nearest empty 5f states.

Figure 1 shows that the spectrum of UGa_2 is similar to UPd_3, with localized $5f^2$ states. Not only are the maxima at very similar energies, 3724.9 and 3725.0 eV, respectively, but they are both similarly narrow. USn_3 with 5f band states occupied by about 2.7 electrons has the maximum at 3724.7 eV, which is not that different as the width, which is affected mainly by the extended high-energy side, indicating a much larger width of unoccupied part of the $5f_{5/2}$ band states. It has been shown previously [36] that USn_3 was partly oxidized, which explains the broadening of the U–M_4 HERFD XAS spectrum.

The shifts of the M_4 edges in metallic systems are smaller than those in uranium oxides—-the latter can be clearly associated with changing the valence and 5f occupation from f^2 to f^0 [U(IV) to U(VI)]. The energy shift of the U–M_4 white line in the HERFD XAS mode for the U(IV) and U(VI) oxides is on the order of 2 eV, while it can vary on a smaller scale (0.2–0.4 eV) depending on details of U environment for various molecular complexes with the same U valence. In case of intermetallic systems, the energy difference between UPd_3 with presumably localized $5f^2$ state and USn_3 close to $5f^3$ is less than 1 eV. A specific feature of metallic systems is the presence of non-f conduction electrons at uranium, which can also contribute by Coulomb repulsion. In other words, changing the uranium valence in oxides changes the number of electrons transferred from uranium to ligand anions, whereas changing the 5f occupancy in metallic systems changes mainly the balance between the U-5f states on one side and U 6d-7s states on the other side. The 5f occupancy variations affect the U-3d energies. The more spatially extended 6d or 7s states may affect the 3d energies less, but the difference is questionable. Aside from the variation of the occupancies of individual states, we can expect that the energy of the 3d states in the ground state can be affected by the 5f delocalization. Extended 5f states should have a lower repulsive interaction to the U-3d shell than localized 5f states, provided equal 5f occupancy. In general, we cannot simply deduce the 5f occupancy from the M-edge energy, which, however, does not mean that inspection of the M-edge energy would be meaningless, as will be shown below.

What can be deduced from the small shift to lower energies from UPd_3 to UGa_2? Considering the effect on the 3d states we would have to assume a higher 5f occupancy. The other effect, the localization, cannot be taken responsible in UGa_2, as the 5f states in UPd_3 *are* already localized. The case of USn_3 is the other reference point, with much higher 5f occupancy (assumed as ≈ 2.7). There is a shift to lower energies, which is perhaps somewhat compensated by the 5f delocalization, yielding 3724.6 eV. The full localization of the $5f^3$ ground state would give appreciably lower energy. On the other hand, the energy shift tells us that the occupancy

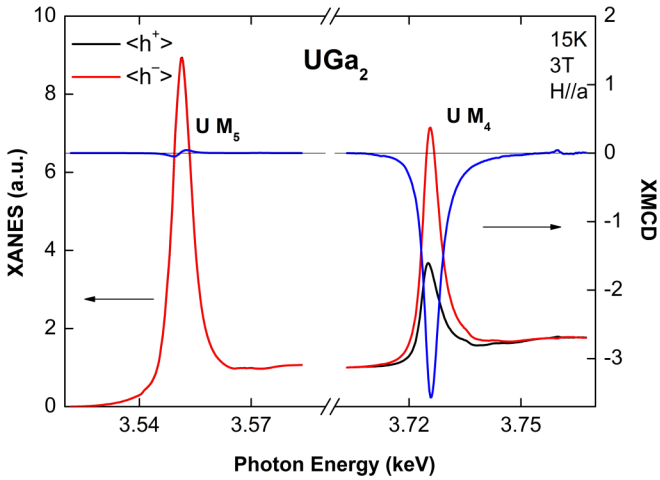

FIG. 2. X-ray absorption at the U–M_5 and M_4 edges for two different helicities (black and red) and the difference of the two helicities (blue).

is most likely higher than 2, and as the noninteger occupancy implies certain delocalization (hybridization), the occupancy cannot be different from 2 by only a small margin—because delocalization means the shift to *higher* energies. Hence we can quite reliably deduce that the HERFD XAS M_4 data indicate a certain delocalization and $5f$ occupancy higher than 2, although not reaching 3, as that would give the edge similar to USn_3. As we will see in Sec. V, a $5f$ occupancy around 2.5 is expected for all DFT methods applied, which is not contradicting the HERFD XAS data. One has to recall at this point that the dominant bandlike character of $5f$ states is evidenced by ultraviolet photoemission spectroscopy (UPS) and $4f$ core-level x-ray photoemission spectroscopy (XPS), exhibiting the $4f$ peaks practically at the same energy as for U metal. The difference is in the existence of high-energy satellites in UGa_2, suggesting an approach to localization [37]. Comparing XPS with HERFD XAS, one actually realizes a remarkable fact that the latter technique can detect smaller energy shifts than $4f$ core-level XPS, despite an order of magnitude higher total energies. The reason is the very sharp white line in HERFD XAS.

Besides the shifts of the M_4 white-line energy, we can try to obtain additional information from the shape of the whole spectrum, being rather diverse, as seen from Fig. 1, especially on the high-energy side. In the case of delocalized wave function of the final state, we can associate the spectrum with the unoccupied part of the appropriate density of states [38], $5f_{5/2}$ for M_4. Its shape and width depend on differences of the $5f$ states occupation, spin-orbit, and exchange splittings as well as on the width of the $5f_{5/2}$ band, reflecting the delocalization of the $5f$ states. We can therefore compare the shape of the M_4 HERFD XAS spectrum with the $5f_{5/2}$ DOS calculated by various theoretical approaches, which can test how much the $5f$ states can be described as itinerant.

B. Uranium M-edge XMCD experiment and preliminary discussion

Figure 2 shows the XANES and XMCD spectra collected at $T = 15$ K in the magnetic field of 3 T for the M_4 and M_5 edges of uranium. The external magnetic field was applied along the a axis, i.e., the easy-magnetization direction, and its intensity is sufficient for saturation of magnetization. The spectra have the characteristics typical for magnetic uranium compounds, with the XMCD M_4 signal forming one negative peak (due to the dominance of spin-down states in unoccupied part of $5f_{5/2}$) and M_5 with both the negative and positive wiggle (as the spin-up and spin-down states largely cancel each other). Integrated intensities at each absorption edge after removal of the transitions to the continuum states give the branching ratio $B = I_{M5}/(I_{M5} + I_{M4}) = 0.697 \pm 0.010$. Applying the spin-orbit sum rule [39], it is possible to determine the expectation value for the angular part of the $5f$ spin-orbit electron operator per hole $\langle w^{110}\rangle/n_h - \Delta$. Knowing n_h, which is the number of $5f$ holes, and considering a small correction term Δ due to exchange interaction with the core hole, one can further obtain the occupation numbers of the $j = 5/2$ and $j = 7/2$ subshells. From the branching ratio, $\langle w^{110}\rangle/n_h - \Delta$ is estimated to be -0.242 ± 0.01, which can be compared to the free ion U^{4+} (-0.200) and U^{3+} (-0.308) derived from relativistic atomic Hartree-Fock calculations in intermediate coupling. This value is a bit smaller than the one reported for UCoGe (–0.252) [40], for which the number of $5f$ electrons is 2.84 according to band-structure calculations [41]. Assuming a linear dependence, the $5f$ count should therefore be close to 2.5, in a good agreement with HERFD XAS measurements, which predict the value between 2 and 3 but not close to either of them. Considering $n_h = 11.5$ and using $\Delta = -0.014$, we obtain the occupation numbers of the subshells $n^{5f}{}_{5/2} = 2.33$ and $n^{5f}{}_{7/2} = 0.17$.

Using the sum rules [42,43], orbital μ_L and spin μ_S U moments can be determined, considering that the number of f holes $n_h = (14–n_f)$ is known and taking the magnetic dipole operator $\langle T_z\rangle$ from atomic multiplets calculations [44]. We obtained $\mu_L = 3.04\,\mu_B$ and $\mu_S = -1.61\,\mu_B$ for $5f^3$, yielding the total moment $\mu_U = 1.43\,\mu_B$. Assuming the $5f^2$ configuration increases the total moment to $\mu_U = 2.20\,\mu_B$, as deduced from $\mu_L = 3.32\,\mu_B$ and $\mu_S = -1.12\,\mu_B$. Considering $n_h = 11.5$ and the linear scaling of $\langle T_z\rangle$ with n_h, we deduce $\mu_L = 3.18\mu_B$ and $\mu_S = -1.31\mu_B$. The obtained total $5f$ magnetic moment of $1.87\mu_B$ is still substantially smaller than the known bulk magnetization of $3.0\mu_B$/U.

It is interesting to point out that polarized neutron diffraction [45] gives moments close to $3.0\,\mu_B$/U, including the suggested diffuse magnetization of 0.22 μ_B parallel to the $5f$ magnetization. Considering possible errors of moments obtained from XMCD, we cannot exclude the influence of surface oxidation, which is ubiquitous to all U-based metallic systems, forming typically a 20–30-nm-thick overlayer of UO_2 upon an air exposure. While such a slab cannot be resolved in any conventional x-ray diffraction experiment, the resonant absorption conditions reduce the effective information depth to the submicrometer range. It means that the contaminated surface can represent over 10% of the probed depth, reducing the obtained moments significantly, as UO_2 being antiferromagnet provides only a very small magnetization in the field of 3 T.

Normalized XANES and XMCD spectra recorded at the K edge of Ga at $T = 15$ K and in magnetic field $\mu_0 H = 3$ T applied along the a axis are presented in Fig. 3. The XMCD

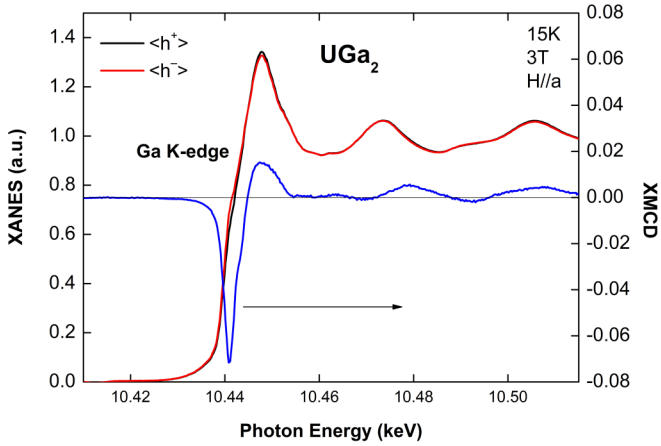

FIG. 3. X-ray absorption at the Ga-*K* edge for two different helicities (black and red) and their difference (blue).

signal at the *K* edge is weak and more intricate to interpret because it is only due to the orbital polarization of the 4*p* states. This polarization is induced both via intra-atomic spin-orbit coupling, if there is a sizable local spin moment on Ga, and via the hybridization of the 4*p* states with spin-orbit split 5*f* states of U. Positive and negative peaks show up at the XMCD Ga *K* edge accordingly [46]. The integration (up to 20 eV above the edge) of those peaks results in a negative signal, i.e., a positive orbital 4*p* moment at the Ga sites. A similar XMCD spectral shape was recorded at the Ge *K* edge in UGe_2 indicating a polarization of the Ge atoms aligned parallel to the uranium magnetic moment [47].

In addition, we performed an x-ray absorption study at high pressures (up to 7.2 GPa) at room temperature (in the total fluorescence yield mode, i.e., not HERFD). Within our experimental detection condition, the white $M_{4,5}$ lines (shown in Fig. 4), each normalized to maximum intensity, are nearly the same irrespective of pressure, meaning that pressure up to 7 GPa has practically no influence on the number of 5*f* holes and on the branching ratio. This correlates with very small changes found in LDA+*U* calculations shown below. A detailed inspection shows a very small shift of M_5 towards higher energies, but the shift is far below the energy resolution and has to be taken with caution.

V. COMPARISON WITH CALCULATIONS

A. Structural parameters and equation of state

The LSDA and GGA approximations to DFT are known to work well for spin magnetism and for well-screened excitations in broadband metals. Problems with the application of LSDA or GGA to narrow 5*f* bands with large orbital magnetic moments were encountered in earlier work on UGa_2. In comparison with the experimental observations, the calculated magnetic moment is too small [8], the Sommerfeld coefficient is too large [6], indicating an overestimated 5*f* density of states at the Fermi level, and the Fermi surfaces do not match the observed de Haas–van Alphen frequencies [6].

Here, the first properties to be addressed are the structure and charge distribution, which are usually both well described by local (LSDA) or semilocal (GGA) approximations. Table I summarizes the results of total energy calculations using the WIEN2K code. The *c*/*a* ratio of UGa_2 with space group 191 was optimized at a number of fixed volumes between 54.4 and 68 $Å^3$ per formula unit, and the resulting energy-volume data were fitted with the Murnaghan equation of state. It turns out that the LSDA total energy at a fixed volume has two local minima as a function of *c*/*a*, one near $c/a \approx 0.65$ and the other at $c/a \approx 0.95$. The latter corresponds to the experimental observations, but for LSDA, the global minimum is found at the smaller ratio and 370 meV per formula unit below the other minimum.

Using the LSDA+*U* changes the relative balance of the two minima and the larger *c*/*a* ratio becomes the global minimum for *U* larger than approximately 1.5 eV. The lattice parameters obtained for $U = 2.0\,\text{eV}$ are in good agreement with experiment and the same holds for the bulk modulus (Table I). We should mention that also GGA+OPC yields a global minimum close to the experimental structure parameters. These

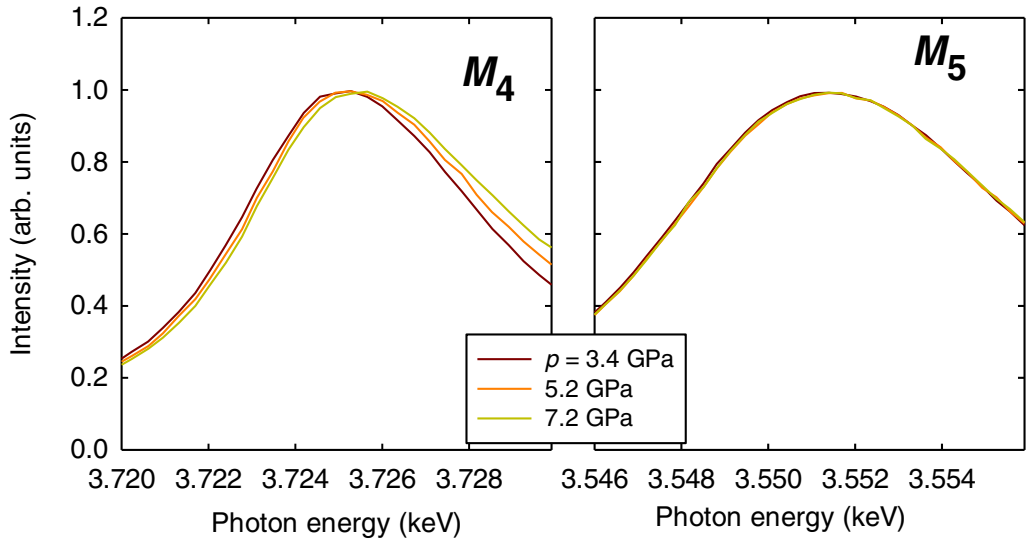

FIG. 4. U–$M_{4,5}$ absorption edges of UGa_2 measured in DAC with increasing hydrostatic pressure.

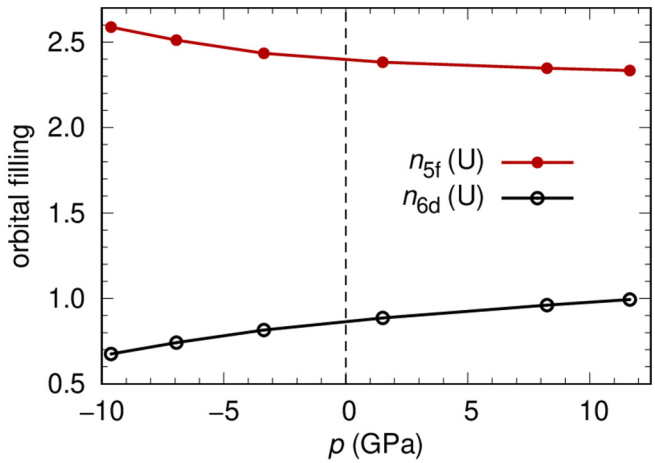

FIG. 5. Variation of the U 5*f* and 6*d* occupancy as a function of pressure (WIEN2K, LSDA+*U* method with $U = 2$ eV). The absolute value of the 6*d* filling is underestimated since only the charge density inside the muffin-tin sphere ($R_{MT} = 2.65\,a_B$) is counted whereas the 6*d* states are delocalized and extend to the interstitial region. In the tight-binding model used for the LDA+DMFT calculations, there are approximately 2 electrons in the uranium-6*d*-like Wannier functions. For comparison, the related FPLO occupation numbers at zero pressure are $n_{6d} = 1.96(1.10)$ for gross (net) occupation, which can be compared with the WIEN2K values of $n_{6d} = 2.0(0.86)$ for total (muffin-tin sphere).

results show that LSDA fails to describe the structure of UGa_2 properly and that an improved approximation is required.

The seemingly counterintuitive finding of two (meta)stable *c*/*a* ratios could have a rational background. Another magnetic system with a simple lattice structure, YCo_5, is known to show an isostructural exchange-driven first-order phase transition under high pressure, which is related to a jump in the *c*/*a* ratio [48]. A possibly similar instability of UGa_2 under high hydrostatic pressure was reported in Ref. [49], where the observed transition at 16 GPa was not isostructural but to a tetragonal phase.

In the context of our experimental investigations of UGa_2 under pressure, it is important to identify trends in the electronic structure as a function of compression. In particular, we explored the stability of the 5*f* and 6*d* occupancies as a function of pressure derived from the computed equation of state (Fig. 5). We see that no dramatic changes of occupancies are envisaged. In principle, we may expect an increase of the 3*d*–5*f* Coulomb repulsion due to volume compression, which is compensated by the reduction of the 5*f* occupancy, so the impact of pressure on the energy of initial state is expected to be small.

B. X-ray absorption spectra

Turning to the spectral properties, it is noted that DFT calculations in general can reproduce energies of core levels within a few percent. For example, using nonmagnetic GGA the FPLO method gives the $3d_{3/2}$ states at ≈ 60 eV lower binding energies (3667 eV) than the experimental energies of the white lines. As a crude approximation of the x-ray absorption process, we may consider how the electronic structure is affected by a 3*d* hole in calculations using a supercell. This static approximation of a 3*d* hole, inducing screening and repopulation of U states, is ignoring the short lifetime of the core hole. Still, such calculations can provide an interesting comparison. When considering one 3*d* hole, the binding energies shift to ≈ 3787 eV, which is now 60 eV higher than the experimental white-line energies. The experimental value is interestingly just in the middle between the ground state and the state with one static 3*d* hole. Such an uncertainty of less than 2% would be very welcome in the low-energy region. It cannot compete, however, with experimental accuracy in the realm of core levels. For this reason, the following comparison between experimental and calculated spectroscopic data will be performed using relative energies or by adjusting the Fermi level.

TABLE II. Measured positions of the ascending-edge inflection points (AE) of U–M_4 edge spectra compared with FPLO occupation numbers and ionicities obtained from nonmagnetic GGA calculations. Both gross and (net) occupation numbers are given, as explained in the Section III B. UPd_3 features two different Uranium positions with accidentally the same ionicity.

Compound	AE (keV)	n_{5f}	n_{6d}	Ionicity
USn_3	3.723 86(10)	2.94 (2.60)	1.95 (1.01)	+0.63
UGa_2	3.724 24(10)	2.63 (2.40)	1.96 (1.10)	+0.90
UPd_3	3.724 43(10)	2.68 (2.39)	1.85 (0.95)	+1.01
		2.74 (2.44)	1.81 (0.94)	+1.01

Figure 1 shows U–M_4 edge spectra of different compounds where the ascending edges of the three metallic systems span a range of 0.57 eV. The question was posed, can the edge positions be used to conclude about the 5*f* occupation numbers, 5*f* delocalization, or other quantities related to the charge distribution? To this end, nonmagnetic GGA calculations for the three metallic systems included in Fig. 1 were carried out and the occupation numbers were extracted from the FPLO population analysis; see Table II. Note that the charge distribution is (and was checked to be) only marginally influenced by magnetic order.

Inspection of Table II shows that the 5*f* occupation of USn_3 is 0.2–0.3 higher than that of UGa_2 or UPd_3, while the latter two show similar numbers. The higher 5*f* occupation of USn_3 meets the expectation. On the other hand, the slightly larger n_{5f} of UPd_3, compared with UGa_2, would contradict the opposite trend in the edge positions. Note that the applied GGA method largely overestimates the hybridization contribution in the case of localized states (the difference between gross and net occupation, i.e., 0.3 electrons in the case of UPd_3). However, a redistribution of the hybridization charge toward localized charge would take place inside the atom and, thus, not essentially change the ionicity. The latter determines the electrostatic potential at the atomic site, hence the position of the core level, with respect to the Fermi energy. Figure 6 illustrates the described relation between ionicity and U–M_4 edge position, which is almost linear for the three available data points.

In the following, results of several electronic structure methods will be compared with experimental results for

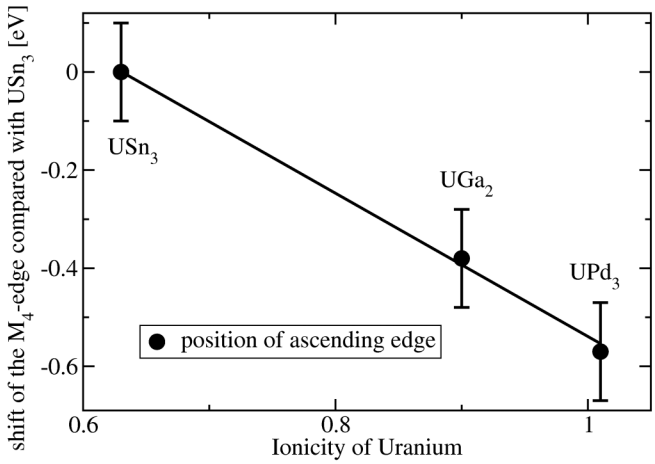

FIG. 6. Shift of the measured ascending edge inflection point vs computed ionicity of the uranium atom in three metallic compounds. The filled circles mark data points; the line is intended to guide the eye.

UGa_2 regarding the line shape of the XAS spectra. Most of these calculations will consider a ferromagnetic ground state. This is self-evident for the low-temperature data collected in the ferromagnetic state. The HERFD-XAS data were however collected at room temperature, where UGa_2 is paramagnetic. Based on the observed large paramagnetic effective moment [6,15] we can assume that the magnetic correlations at about $2 \times T_C$ exist on much longer timescale comparing to the electronic (hopping) scale. In order to model the effects of intrashell polarization in the DFT framework, it is thus appropriate to simulate the paramagnetic state with a static, ordered state. For simplicity, we have chosen a ferromagnetic state.

Figures 7 and 8 present a comparison between the HERFD XAS data and several calculated densities of U-$5f_{5/2}$ states combined with appropriate inverse Fermi distribution ($T = 300$ K), Lorentzian broadening of 0.4 eV full width at half maximum to simulate the finite lifetime of the core hole, and an additional Gaussian broadening of 0.8 eV FWHM. The latter value was chosen to reproduce the width of the main peak in the measured XAS for the average of the calculated spectra; see Fig. 8.

The experimental spectrum (the same data as in Fig. 1) shows a single peak with a FWHM of 1.7 eV, a shoulder at around 2 eV above the maximum, and a tail toward higher energy. The nonmagnetic GGA data have a two-peak structure before broadening (not shown) due to mixing of atomic $5f_{5/2}$ and $5f_{7/2}$ states by the ligand field, but the distance between these peaks amounts to 0.75 eV only. The resulting broadened curve (Fig. 8) has a FWHM of only 1.1 eV and lacks any visible shoulder. Additional mixing is provided by the exchange interaction in the ferromagnetic GGA calculation, yielding a very similar FWHM as the experimental main peak, but a much smaller intensity in the shoulder and tail region. If the orbital polarization is taken into account in GGA-OPC, the six m_j channels receive an additional splitting, where m_j denotes the magnetic quantum number. This results in a separation of about 1.5 eV between the two peaks. While this separation almost meets the experimental distance between the main peak and the shoulder, the intensity relations are different: the calculated shoulder is too high and the calculated tail too small.

The ferromagnetic GGA and GGA+OPC reproduce important features of the experimental spectrum, but not to a satisfactory amount. This could be related to either of the two implicit assumptions (i) a ferromagnetic state would model the situation at room temperature and (ii) a semilocal (+OPC) approximation would reasonably account for the excited-state properties.

Both assumptions can be checked by comparing the experiment with LDA+DMFT, where many-body excitations in and about the 5*f* shells are embedded into the DFT framework and where the paramagnetic state is accessible as well. The ferromagnetic LDA+DMFT* data are shown in the rightmost part of Fig. 7 and in Fig. 8. Both the shoulder and

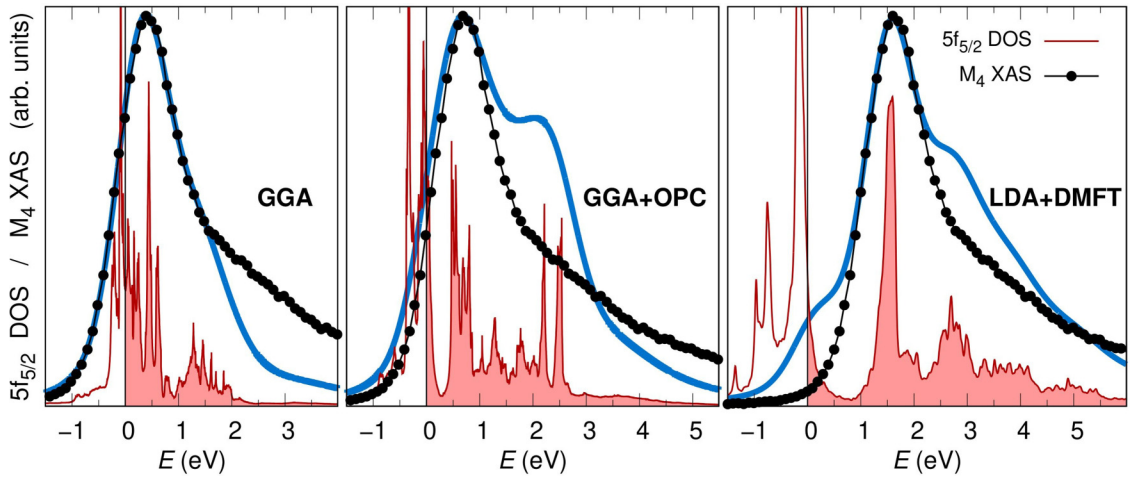

FIG. 7. Calculated M_4 spectra (thick blue lines) obtained by broadening the *j*-resolved densities of states ($5f_{5/2}$–red) corresponding to ferromagnetic solutions from GGA (FPLO, left), GGA+OPC (FPLO, middle), and LDA+DMFT* (right). The black lines with dots represent the experimental data from HERFD XAS (the same as shown in Fig. 1). The experimental spectrum was aligned with the theoretical main peak.

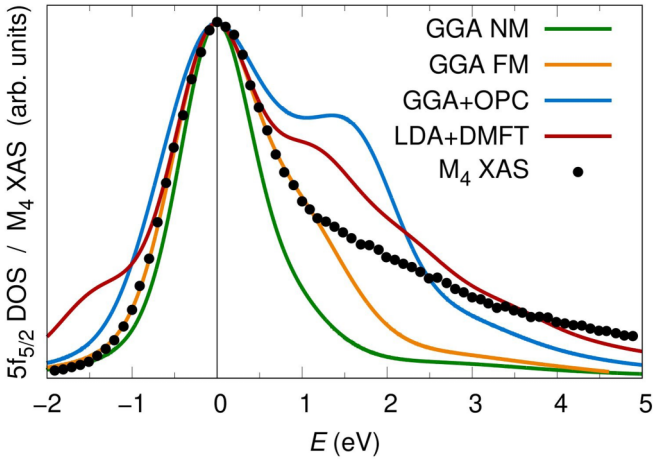

FIG. 8. Comparison of all calculated M_4 spectra (full lines) with the experimental HERFD XAS data (dots). All data are the same as in Fig. 5, but nonmagnetic GGA is added. The main peaks of all datasets are aligned.

the tail are closer in intensity to the experiment than in the GGA+OPC case. However, there is an additional shoulder at the Fermi level that is not present in the experiment or in any of the other calculations. We attribute this feature to a slight inconsistency between the 5*f* filling computed in the auxiliary impurity model and the filling evaluated from the reciprocal-space integral (the former being larger), which is due to the approximate (sparsely discretized) hybridization function. This inconsistency shifts the Fermi level down to states that should otherwise be occupied and thus invisible to XAS. To identify the individual spectral features, an analysis of the many-body eigenstates of the impurity model would be needed, which is computationally prohibitive. Nevertheless, it turns out that removing the hybridization and the crystal field from the impurity model has only a minor effect on the XAS spectrum—-and the resulting *paramagnetic* atomic model is accessible to a detailed analysis. The XAS final states correspond to the $5f^4$ configurations. The main peak of the XAS spectrum is due to the $5f^4$ ground state ($J = 4, L \approx 6, S \approx 2$). The dominant contribution to the shoulder comes from two excited states that are mixtures of configurations with $S = 2$ (all four electrons aligned) and $S = 1$ (one of the electrons flipped).

To summarize the comparison of theoretical and experimental XAS line shapes, the intra-atomic magnetic correlations seem to be indispensable to explain the width of the main peak without the need of unrealistic broadening. The shoulder and the tail are probably due to the excitations to higher atomic multiplets of the $5f^4$ configuration. GGA+OPC can partly model this situation but it yields a downshift of the spectral weight from the tail region toward the shoulder. LDA+DMFT* shows a more realistic distribution of the spectral weight on the high-energy side.

C. Magnetic moments and occupation numbers

We now show and discuss the results for 5*f* occupation numbers, magnetic moments, Sommerfeld parameter, and branching ratio, listed and compared with the experimental values in Table III. Before considering the individual quantities, we compare LSDA results obtained by the WIEN2K code with those obtained by FPLO. Within these two datasets, the occupation numbers, the uranium spin and orbital moments, and the branching ratio differ only marginally, i.e., in the last digit. This is particularly remarkable for the case of the 5*f* occupation numbers, since the projections of WIEN2K (onto real-space domains or Wannier functions) and FPLO (onto local orbitals) are different. Nonetheless, the number for muffin-tin sphere projection is almost the same as that for net projection; the same holds for Wannier vs gross projections. A significant difference is present for the unit-cell total moment, obviously due to differences in the interstitial region. A larger difference of about 20% is found for the Sommerfeld parameter, which is proportional to the DOS at the Fermi level. In a mathematical language, the DOS is a distribution and its numerical value at the Fermi level can be sensitive to small details of the band structure. Thus, it is not expected to find much better agreement among two different methods. All in all, we find a reassuringly good agreement between both codes, in accordance with previous findings regarding elastic properties [50].

All applied theoretical methods find the 5*f* occupation of 2.5–2.6 (see Table III) if muffin-tin or net occupations are evaluated, which can be considered as "localized" contributions to the 5*f* manifold. A 5*f* count of about 2.5 was indeed anticipated in the preliminary discussion of the XMCD experiment, Sec. IV B. If Wannier or gross occupations are considered, the numbers amount to 2.7–2.8, i.e., the hybridization contributions are close to 0.2 electrons for all methods. This very small sensitivity of occupation numbers with respect to the theoretical method can be understood by the dominant role of the static charge distribution among the relevant energy scales (Hartree energy).

We now turn to the spin contribution to the magnetic moment. Here and for the discussion of other data being sensitive to the magnetic state, we disregard the LDA+DMFT results, which are obtained without exchange coupling among uranium 5*f* and 6*d* states. Adding the empirically estimated exchange splitting of 35 meV to the 5*f* shell increases the moments quite substantially; see the last line of Table III. This approach, termed LDA+DMFT*, and the other theoretical methods find uranium spin moments ranging from 1.9 μ_B (LSDA and LDA+DMFT*), 2.0 μ_B (GGA), 2.3 μ_B (GGA+OPC) to 2.4 μ_B (LSDA + U = 2 eV). While the spread is larger than among the occupation numbers, it amounts to not much more than 10% around its barycenter.

For the discussion of the orbital magnetic moment, we disregard the data obtained by LSDA, GGA, and LSDA+U, which are all known for deficiencies in the description of orbital magnetism, as outlined above. The two remaining methods, GGA+OPC and LDA+DMFT*, agree in the value of the uranium orbital moment, 4.6 μ_B.

The total unit-cell moment is almost identical to the total uranium moment, since small Ga moments and diffuse contributions compensate each other. The calculated GGA+OPC value of 2.3 μ_B is 22% smaller than the experimentally determined macroscopic magnetization of 3.0 μ_B/U. A possible reason for this difference could be an overestimation of the spin moment in the collinear implementation of GGA+OPC

in the FPLO code. The total unit-cell moment of $2.8\,\mu_B$ obtained by LDA+DMFT* is still somewhat smaller than the experimental value, but close to the experimental error bar $\pm 0.1\,\mu_B$. The ratio of the orbital to spin moment, 2.0 for GGA+OPC and 2.5 for LDA+DMFT*, lies within the experimental range for both methods.

We now turn our attention to the Sommerfeld parameter γ. It is clearly overestimated in LSDA. A better description of exchange and correlation reduces its value, which is mainly due to a shift of the occupied 5f states from the Fermi level to higher binding energies. The most reliable estimates should be provided by those two methods that are not under suspicion to underestimate the orbital moment, with related distortions of the electronic DOS. The experimental value, 11 mJ/mol K^2, is larger than the value obtained by LDA+DMFT* and smaller than the GGA+OPC result, both deviating by about 30% from experiment. Given the discussed numerical difficulty to obtain precise values of DOS, such a difference appears to be justifiable, i.e., it is only marginally significant.

An interesting point to note is the factor of 2 difference in the Sommerfeld parameter obtained by LSDA and GGA calculations. Inspection of the DOS (not shown here) makes it clear that this is due to a slightly larger uranium spin moment in the GGA calculation (by about $0.1\,\mu_B$). Such a little difference yields a larger splitting of the spin channels on the order of 0.1 eV. This way, the Fermi level becomes situated in a region of relatively low DOS in the GGA calculation while it is placed on a slope in LSDA. This example shows the strong sensitivity of low-energy properties like Sommerfeld parameter or de Haas–van Alphen data with respect to details of the DFT model used, particularly in the case of narrow-band systems and in the presence of magnetism.

Finally, we consider the branching ratio, which amounts to $B = 0.697$ according to the present experiment with an error bar of about ± 0.010. Since the present calculations neglect core-hole effects, we use $\Delta = 0$ to evaluate the theoretical values of B. The local (LSDA) and semilocal (GGA) approximations yield too-small values of $B = 0.67$, which can be understood in terms of an overestimated band dispersion. In the limit of very large dispersion, the branching ratio would tend to 0.6, while in the opposite limit of vanishing dispersion, it would tend to 1.333 for uranium. Application of LSDA+U enhances B to 0.68, which is still somewhat smaller than its experimental value. Only the two methods that include an appropriate modeling of the orbital magnetism also provide values of the branching ratio close to the experimental range (considering the error bar): GGA+OPC with $B = 0.685$ and LDA+DMFT* with $B = 0.71$.

Summarizing the comparison of experiment with theoretical calculations, both the GGA+OPC and the LDA+DMFT* methods yield a decent, though not excellent, description of the M_4 HERFD XAS spectral shape. The results of both methods also agree, within or at least close to the error bars, with the experimental branching ratio, the Sommerfeld parameter, and the ratio between uranium orbital and spin magnetic moments. The GGA+OPC method underestimates the total magnetic moment by 22%, which is consistent with a possible overestimation of the band dispersion (bandwidth) already discussed above in the context of the GGA approximation. The total moment obtained by LDA+DMFT* is only 7% smaller than its experimental counterpart and, thus, can be considered to give a good account of the available experimental information. A reason for the remaining slight underestimation of the magnetic moments could be their sensitivity to the ligand-field splitting, which is due to the crystal electric field as well as due to hybridization. Since our discrete representation of the hybridization is a rather crude approximation in metallic systems like UGa_2, some inaccuracy of the computed crystal-field splitting has to be expected.

VI. CONCLUDING REMARKS

Our XAS spectroscopy study did not provide sufficient evidence for a clear characterization of the 5f localization/delocalization or the actual 5f occupancy. However, it can

TABLE III. Computed properties of the in-plane ferromagnetic state at the experimental lattice geometry. The magnetization was assumed along [100], the a axis, except for the LDA+DMFT calculations where it was assumed along [210], the b axis. From left to right: filling of the uranium 5f states (WIEN2K: numbers without parentheses are from the muffin-tin spheres, numbers in parentheses are from Wannier functions; FPLO: the first numbers refer to net and the second to gross occupations), uranium orbital (μ_L), spin (μ_S), and total (μ_{tot}) magnetic moments (net contributions in the case of FPLO), the total magnetic moment of the unit cell, the Sommerfeld coefficient, and the M-edge branching ratio. The difference between the uranium total moment and the unit-cell total moment comes from the spin moment residing in the interstitial region of the LAPW basis (WIEN2K, where the magnetic moment at the gallium atoms is negligible, Ga $\mu_{tot} \cong 0.01\,\mu_B$), or from minor contributions at the Ga sites (FPLO).

Method	U n_{5f}	U μ_L (μ_B)	U μ_S (μ_B)	$\lvert U\mu_L/U\mu_S\rvert$	U μ_{tot} (μ_B)	μ_{tot} (μ_B)	γ (mJ/mol K^2)	B
LSDA, WIEN2K	2.51(2.72)	2.70	–1.91	1.42	0.80	0.58	25	0.670
LSDA, FPLO	2.47(2.68)	2.70	–1.90	1.42	0.80	0.69	29	0.672
GGA, FPLO	2.47(2.68)	2.69	–2.02	1.33	0.67	0.56	15	0.670
GGA+OPC, FPLO	2.57(2.73)	4.64	–2.26	2.05	2.38	2.33	15	0.685
LSDA+U (1 eV), WIEN2K	2.54	4.25	–2.17	1.96	2.08	1.86	10	0.682
LSDA+U (2 eV), WIEN2K	2.58	4.70	–2.37	1.98	2.33	2.12	15	0.677
LDA+DMFT	(2.80)	(2.92)	(–1.16)	(2.52)	(1.76)	1.76	12	0.711
LDA+DMFT*	(2.76)	(4.60)	(–1.85)	(2.49)	(2.75)	2.75	8	0.709
Experiment				1.9–3.0		3.0 [5]	11 [5]	0.697

single out those situations which are entirely implausible. We can exclude the localized f^2 as well as completely localized f^3 behavior, but the HERFD XAS data do not allow for a decision between situations close to the f^2 localized state or a partly delocalized state close to f^3, mainly due to the lack of HERFD XAS data on well-characterized U intermetallic references. Despite these limitations, a putative linear relation could be established between the U–M_4 edge positions and the calculated uranium ionicities of three intermetallic compounds.

The experimental bulk moment of 3.0 μ_B/f.u. was not reproduced by XMCD (suggesting otherwise the 5*f* occupancy close to 2.5), which gives only about half of the bulk value, but we cannot exclude a certain influence of surface oxidation, or even effects of surface polishing yielding a noncollinear ferromagnetic arrangement in the topmost atomic layers. However, the 5*f* occupancy close to 2.5 suggested by the XMCD data agrees with the localized contributions to the 5*f* occupation numbers obtained in all computational approaches we applied.

The XAS spectra clearly suggest a necessity of atomic multiplets to be included in the theoretical modeling. Considering also thermodynamic data, we encounter a rather special situation: the Sommerfeld coefficient amounts to only 11 mJ/mol K^2, suggesting a small 5*f* contribution to the electronic density of states at the Fermi level, while photoemission shows 5*f* states at or very close to E_F. This is true for historical UPS spectra on polycrystalline films [10] as well as for new high-resolution soft x-ray photoemission spectra on single crystals [37].

Other existing spectroscopy data, namely XPS, can also be tentatively linked with HERFD XAS data, as they can help to separate the effects of a deep core state from the properties of available empty electronic states. The 3*d* core-level spectra in actinides are not studied routinely, being far beyond the energy range of common XPS instrumentation. However, we can get at least a qualitative estimate from the available U-4*f* spectra; see, e.g., Ref. [37] and references therein. The energies of the $4f_{5/2}$ and $4f_{7/2}$ lines in UGa_2, 387.99 and 377.18 eV [10], are by ≈0.3 eV higher than in U metal and are slightly lower than in UN, where a certain loss of the 5*f* charge can be expected due to the N bonding [51,52]. These data indicate that UGa_2 has less 5*f* electrons than U metal and they are in the same time more localized.

One should stress that in the case of U-4*f* XPS spectroscopy, the shifts of the spectral lines in intermetallics are much smaller than in UO_2, where the 4*f* lines shift by 3 eV towards higher energies compared with U metal [53]. This shift is much larger than in XAS, which can be related to the lack of 5*f* screening of the 4*f* hole in XPS [54]. In the charge-neutral XAS, the screening 5*f* electron is provided by the process itself and does not need to be transferred from neighbor atoms (which is not possible on the timescale of the XPS experiment).

The lack of *f* screening can be also taken responsible for the main XPS 4*f* lines in UPd_3, where the $4f_{7/2}$ peak is found at 378.8 eV. However, its shoulder at 377.2 eV, which can be associated with a 5*f*-screened final state, is practically equivalent to the related main-peak energy in UGa_2 [55], only its lower intensity compared to UGa_2 indicates that the probability of 5*f* screening is much lower, due to the smaller hybridization (i.e., smaller hopping rate) in UPd_3 than in UGa_2.

We can conclude that the spectroscopic and thermodynamic data in comparison with calculations of various kinds indicate that the 5*f* states in UGa_2, although not fully localized, are strongly affected by atomic multiplet effects, which are not well described by LSDA or GGA. A better model was found to be GGA+OPC, where the orbital polarization of the atomic states is embedded in a Kohn-Sham scheme. Yet better, though not without room for further improvement, was the description provided by a particular LDA+DMFT implementation.

So far, the strongly correlated *f* systems were investigated mainly in the context of heavy fermions. UGa_2 is a strongly correlated low-γ material, though the 5*f* states are observed close to the Fermi level in photoelectron spectroscopies. The size of the magnetic moment in the ferromagnetic phase is interestingly higher than results of all computational approaches applied so far, which can signal that some part of physics is being overlooked by these theoretical methods.

It is naturally useful to seek analogies among U systems. A combination of large moments and low-γ value has been observed among metallic U systems, e.g., in UPdSn, an ordered ternary compound with crystal structure similar to that of UGa_2, which has an antiferromagnetic ground state and $\gamma = 5$ mJ/mol K^2 [56]. First suspected of exhibiting 5*f* localization, existing photoelectron spectroscopy data show some of the 5*f* states near E_F [57,58]. In comparison to UGa_2, the ordered moments are lower, reaching only ≈2.0 μ_B/U.

ACKNOWLEDGMENTS

This work was supported by the Czech Science Foundation under Grants No. 18–02344S and No. 21–09766S. K.O.K. acknowledges support by European Research Council under Horizon 2020 Framework Programme (H2020) - ERC grant No. 759696. We thank Patrick Colomp of the Radioprotection services for his help at ID26 and ID12 beamlines of ESRF, Ulrike Nitzsche for maintaining the high-performance computing environment at IFW Dresden, and Shin-ichi Fujimori for fruitful discussion. During the final processing of the present paper, a separate theory article [59] has been published, which brings more details on the DFT+DMFT calculations of UGa_2.

[1] Y. Baer, H. R. Ott, and K. Andres, Solid State Commun. **36**, 387 (1980).

[2] K. Andres, D. Davidov, P. Dernier, F. Hsu, W. A. Reed, and D. J. Nieuwenhuys, Solid State Commun. **28**, 405 (1978).

[3] A. Andreev, V. K. Belov, A. Deriagin, V. Z. A. Kazei, R. Z. Levitin, A. Menovsky, Y. F. Popov, and V. I. Silant'ev, Sov. Phys. JETP **48**, 1187 (1978).

[4] A. C. Lawson, A. Williams, J. L. Smith, P. A. Seeger, J. A. Goldstone, J. A. O'Rourke, and Z. Fisk, J. Magn. Magn. Mater. **50**, 83 (1985).

[5] J.-M. Fournier and R. Troc, in *Handbook on the Physics and Chemistry of the Actinides*, edited by A. J. Freeman, and G. H. Lander (North-Holland, Amsterdam 1985), Vol. 2, p. 35.

[6] T. Honma, Y. Inada, R. Settai, S. Araki, Y. Tokiwa, T. Takeuchi, H. Sugawara, H. Sato, K. Kuwahara, M. Yokoyama, H. Amitsuka, T. Sakakibara, E. Yamamoto, Y. Haga, A. Nakamura, H. Harima, H. Yamagami, and Y. Ōnuki, J. Phys. Soc. Jpn. **69**, 2647 (2000).

[7] L. M. da Silva, A. O. dos Santos, A. N. Medina, A. A. Coelho, L. P. Cardoso, and F. G. Gandra, J. Phys.: Condens. Matter **21**, 276001 (2009).

[8] M. Diviš, M. Richter, H. Eschrig, and L. Steinbeck, Phys. Rev. B **53**, 9658 (1996).

[9] R. J. Radwanski and N. H. Kim-Ngan, J. Magn. Magn. Mater. **140–144**, 1373 (1995).

[10] T. Gouder, L. Havela, M. Divis, J. Rebizant, P. M. Oppeneer, and M. Richter, J. Alloys Compd. **314**, 7 (2001).

[11] A. V. Kolomiets, J.-C. Griveau, J. Prchal, A. V. Andreev, and L. Havela, Phys. Rev. B **91**, 064405 (2015).

[12] C. Gauthier, V. A. Sole, R. Signorato, J. Goulon, and E. Moguiline, J. Synchrotron Radiat. **6**, 164 (1999).

[13] P. Glatzel and U. Bergmann, Coord. Chem. Rev. **249**, 65 (2005).

[14] K. O. Kvashnina and A. C. Scheinost, J. Synchrotron Radiat. **23**, 836 (2016).

[15] A. Rogalev, J. Goulon, C. Goulon-Ginet, and C. Malgrange, *Magnetism and Synchrotron Radiation (Lecture Notes in Physics vol 565)* edited by E. Beaurepaire, F. Scheurer, G. Krill, and J. P. Kappler (Springer-Verlag, Berlin, 2001), pp. 60–86.

[16] F. Wilhelm, N. Jaouen, A. Rogalev, W. G. Stirling, R. Springell, S. W. Zochowski, A. M. Beesley, S. D. Brown, M. F. Thomas, G. H. Lander, S. Langridge, R. C. C. Ward, and M. R. Wells, Phys. Rev. B **76**, 024425 (2007).

[17] M. J. Berger, J. H. Hubbell, S. M. Seltzer, J. Chang, J. S. Coursey, R. Sukumar, D. S. Zucker, and K. Olsen (2010), https://www.nist.gov/pml/xcom-photon-cross-sections-database.

[18] F. Wilhelm, J.-P. Sanchez, and A. Rogalev, J. Phys. D: Appl. Phys. **51**, 333001 (2018).

[19] F. Wilhelm, G. Garbarino, J. Jacobs, H. Vitoux, R. Steinmann, F. Guillou, A. Snigirev, I. Snigireva, P. Voisin, D. Braithwaite, D. Aoki, J. P. Brison, I. Kantor, I. Lyatun, and A. Rogalev, High Pressure Res. **36**, 445 (2016).

[20] F. Zhou and V. Ozoliņš, Phys. Rev. B **80**, 125127 (2009).

[21] O. Eriksson, B. Johansson, and M. S. S. Brooks, J. Phys.: Condens. Matter **1**, 4005 (1989).

[22] H. Eschrig, M. Sargolzaei, K. Koepernik, and M. Richter, Europhys. Lett. **72**, 611 (2005).

[23] G. Jomard, B. Amadon, F. Bottin, and M. Torrent, Phys. Rev. B **78**, 075125 (2008).

[24] P. Blaha, K. Schwarz, F. Tran, R. Laskowski, G. K. H. Madsen, and L. D. Marks, J. Chem. Phys. **152**, 074101 (2020); D. D. Koelling, and B. N. Harmon, J. Phys. C: Solid State Phys. **10**, 3107 (1977).

[25] J. P. Perdew and Y. Wang, Phys. Rev. B **45**, 13244 (1192).

[26] J. Kolorenč, A. B. Shick, and A. I. Lichtenstein, Phys. Rev. B **92**, 085125 (2015).

[27] J. Kuneš, R. Arita, P. Wissgott, A. Toschi, H. Ikeda, and K. Held, Comput. Phys. Commun. **181**, 1888 (2010).

[28] A. A. Mostofi, J. R. Yates, Y.-S. Lee, I. Souza, D. Vanderbilt, and N. Marzari, Comput. Phys. Commun. **178**, 685 (2008).

[29] H. Ogasawara, A. Kotani, and B. T. Thole, Phys. Rev. B **44**, 2169 (1991).

[30] A. B. Shick and A. I. Lichtenstein, J. Magn. Magn. Mater. **454**, 61 (2018).

[31] L. Peters, I. Di Marco, P. Thunström, M. I. Katsnelson, A. Kirilyuk, and O. Eriksson, Phys. Rev. B **89**, 205109 (2014).

[32] M. S. S. Brooks and B. Johansson, J. Phys. F: Met. Phys. **13**, L197 (1983).

[33] L. V. Pourovskii, G. Kotliar, M. I. Katsnelson, and A. I. Lichtenstein, Phys. Rev. B **75**, 235107 (2007).

[34] K. Koepernik and H. Eschrig, Phys. Rev. B **59**, 1743 (1999); https://www.fplo.de/.

[35] J. P. Perdew, K. Burke, and M. Ernzerhof, Phys. Rev. Lett. **77**, 3865 (1996).

[36] K. O. Kvashnina, H. C. Walker, N. Magnani, G. H. Lander, and R. Caciuffo, Phys. Rev. B **95**, 245103 (2017).

[37] S.-I. Fujimori, M. Kobata, Y. Takeda, T. Okane, Y. Saitoh, A. Fujimori, H. Yamagami, Y. Haga, E. Yamamoto, and Y. Onuki, Phys. Rev. B **99**, 035109 (2019).

[38] T. K. Sham, Phys. Rev. B **31**, 1888 (1985).

[39] G. van der Laan, K. T. Moore, J. G. Tobin, B. W. Chung, M. A. Wall, and A. J. Schwartz, Phys. Rev. Lett. **93**, 097401 (2004).

[40] M. Taupin, J. P. Sanchez, J. P. Brison, D. Aoki, G. Lapertot, F. Wilhelm, and A. Rogalev, Phys. Rev. B **92**, 035124 (2015).

[41] M. Samsel-Czekala, S. Elgazzar, P. M. Oppeneer, E. Talik, W. Walerczyk, and R. Troć, J. Phys.: Condens. Matter **22**, 015503 (2010).

[42] B. T. Thole, P. Carra, F. Sette, and G. van der Laan, Phys. Rev. Lett. **68**, 1943 (1992).

[43] P. Carra, B. T. Thole, M. Altarelli, and X. Wang, Phys. Rev. Lett. **70**, 694 (1993).

[44] G. van der Laan and P. T. Thole, Phys. Rev. B **53**, 14458 (1996).

[45] R. Ballou, A. V. Deriagin, F. Givord, R. Lemaire, R. Z. Levitin, and F. Tasset, J. Phys. Colloques **43**, C7-279 (1982).

[46] V. N Antonov, B. N. Harmon, and A. N. Yaresko, J. Phys.: Condens. Matter **19**, 186222 (2007).

[47] Y. Inada, T. Honma, N. Kawamura, M. Suzuki, H. Miyagawa, E. Yamamoto, Y. Haga, T. Okane, S.-i. Fujimori, and Y. Ōnuki, Physica B **359–361**, 1054 (2005).

[48] H. Rosner, D. Koudela, U. Schwarz, A. Handstein, M. Hanfland, I. Opahle, K. Koepernik, M. D. Kuz'min, K.-H. Müller, J. A. Mydosh, and M. Richter, Nat. Phys. **2**, 469 (2006).

[49] N. R. Sanjay Kumar, N. Subramanian, N. V. Chandra Shekar, M. Sekar, and P. Ch. Sahu, Philos. Mag. Lett. **84**, 791 (2004).

[50] K. Lejaeghere, G. Bihlmayer, T. Björkman, P. Blaha, S. Blügel, V. Blum, D. Caliste, I. E. Castelli, S. J. Clark, A. Dal Corso *et al.*, Science **351**, aad3000 (2016).

[51] M. S. S. Brooks, J. Phys. F: Metal Phys. **14**, 639 (1984).

[52] L. Havela, F. Wastin, J. Rebizant, and T. Gouder, Phys. Rev. B **68**, 085101 (2003).

[53] M. Eckle and T. Gouder, J. Alloys Compd. **374**, 261 (2004).

[54] J. C. Fuggle, M. Campagna, Z. Zolnierek, R. Lässer, and A. Platau, Phys. Rev. Lett. **45**, 1597 (1980).

[55] S.-i. Fujimori, Y. Takeda, T. Okane, Y. Saitoh, A. Fujimori, H. Yamagami, Y. Haga, E. Yamamoto, and Y. Ōnuki, J. Phys. Soc. Jpn. **85**, 062001 (2016).

[56] F. R. de Boer, E. Brück, H. Nakotte, A. V. Andreev, V. Sechovský, L. Havela, P. Nozar, C. J. M. Denissen, K. H. J. Buschow, B. Vaziri, P. Meissner, H. Maletta, and P. Rogl, Physica B **176**, 275 (1992).

[57] L. Havela, T. Almeida, J. R. Naegele, V. Sechovský, and E. Brück, J. Alloys Compd. **181**, 205 (1992).

[58] J.-S. Kang, S. C. Wi, J. H. Kim, K. A. McEwen, C. G. Olson, J. H. Shim, and B. I. Min, J. Phys.: Condens. Matter **16**, 3257 (2004).

[59] B. Chatterjee and J. Koloren, Phys. Rev. B **103**, 205146 (2021).